




Enhancing Thermal Performance and Lifetime Cycles of Li-ion Battery in Electric Vehicles

Karim Mostafa Fayez*[‡] , Mohamed Abdul Raouf Shafei* , Doaa Khalil Ibrahim* 

* Department of Electrical Power Engineering, Faculty of Engineering, Cairo University, Giza, Egypt.

(eng.karim_fayez@yahoo.com, mohamed.shafei@eng.cu.edu.eg, doaakhalil73@eng.cu.edu.eg)

‡ Corresponding Author; Karim Mostafa Fayez, Department of Electrical Power Engineering, Faculty of Engineering, Cairo University, Giza, Egypt.

Tel: +201144527033, eng.karim_fayez@yahoo.com

Received: xx. xx. xxxx Accepted: xx. xx. xxxx

Abstract — Hybrid energy storage system has essential priority in Electric Vehicle applications. Therefore, the design of an appropriate power sharing algorithm among energy storage components is necessary to improve battery thermal performance and provide extra extension of battery lifetime cycles. This paper presents an analytical study on the effect of using wavelet decomposition-based power sharing algorithm to force the high frequency component to be fed by the supercapacitor and accordingly reduces the thermal stress on the battery. The proposed approach was investigated by applying it on electric vehicle model in ADVISOR Tool/MATLAB using different driving profiles such as Urban Dynamometer Driving Schedule profile, Highway Fuel Economy Test, New York City Cycle, Los Angeles 1992 and new European driving cycle. The results declare that by using proposed power sharing algorithm, the working temperature of lithium battery decreases significantly while battery lifetime cycles increase, apparently. For urban dynamometer driving schedule, the operating temperature of lithium battery is improved much at maximum decomposition levels reaching to only 25.6 °C compared to 35 °C. In addition, the battery lifetime cycles increased from 2213 to 2585 cycles. Neural Networks pattern recognition tool is also applied to classify the driving cycle to the nearest reference cycles chosen to represent the different driving conditions which help to detect the appropriate wavelet decomposition level, achieving better battery thermal performance and battery lifetime cycles.

Keywords: Battery lifetime cycles, Battery thermal performance, Electric Vehicle, Hybrid Energy Storage System, Lithium Battery, Wavelet Transform.

1. Introduction

By 2050, the number of cars and trucks worldwide has been expected to exceed 2.5 billion. All these amounts of vehicles will consume massive fuels. Therefore, alternative fuels, particularly for urban transportation, are the most pressing demands of our time [1]. Electric traction sector is one of the most growing sectors all over the world as a vital service to reduce transport sector energy and emissions [2], [3].

Batteries, which are part of energy storage system for electric vehicles (EVs), are exposed to harmful, sudden, and high discharging currents because of transient demand power in acceleration and deceleration [4], [5]. In addition, they are exposed to abrupt high charging currents during regenerative braking (RB) which increase the thermal stress on batteries and affect their battery lifetime cycles [5], [6]. Accordingly, it becomes an essential target to overcome the problem of aging and degradation of batteries because of transient demand of power at sudden acceleration and deceleration beside the acquisition of RB power. One of the most practical solutions to overcome the transient demand

of power for EV is to apply hybrid energy storage system (HESS) approaches. In general, several HESSs in vehicular applications have been studied in the past few decades, such as Battery-Supercapacitor (SC), Battery-Superconducting Magnetic Energy Storage, Fuel Cells-SC and Fuel Cells-Battery-SC combination.

Because of the significant benefits of SC as high-power density, less maintenance, large number of operation cycles and less sensitive to temperature variation [6], HESSs of battery-SC have been implemented in several reported studies. In fact, the effectiveness of using SCs in HESS was justified experimentally for urban commercial vehicles on standard driving cycles in [7]. The achieved results have shown that SCs can improve the expected battery lifespan with maximum effectiveness up to 52% for driving patterns without negative road slopes.

In [8], HESSs of battery-SC were used with four different semi-active topologies, while SC size was optimized by dynamic programming (DP) approach. HESS sizing optimization and complete analysis for battery-SC HESS

using DP approach to minimize vehicle lifetime costs was also presented in [9]. It refers to the main factor affects the EV cost is battery degradation whose impact index reaches to 89% of HESS costs among eight sensitive factors: driving cycle, driving range, HESS topology, bus voltage, DC/DC conversion efficiency, battery price, SC price and DC/DC converter price.

Actually, the configuration of HESS calls the need to develop effective power sharing algorithm (PSA) to determine the amount of energy to be fed by different components of HESS. The most common approaches applied for power sharing of HESSs are: look-up tables [10], rule-based approaches [11], fuzzy logic techniques [12], optimization approaches [5], filtration-based techniques rely on Fourier as in [13] and wavelet transform (WT) which was also applied in [14], [15] and [16].

For HESS comprises two different battery technologies, a PSA based on look-up table approach is used in [10] to distribute the power delivered by each battery depending on its state of charge (SOC). The strategy allocates the power between sodium-ion and lithium-ion by specifying power allocation factors determined based on different SOC of batteries. Despite such a strategy providing a good allocation in different operation modes, but it does not take into consideration the aging effect of batteries in case of extreme variations in power demand. The major disadvantage is that RB is limited to be absorbed under specific SOC. However, if SC is used, it can absorb RB whatever the SOC of SC is, and until reaching 100% SOC. Determining the appropriate discharging current from SC using an advanced rule-based PSA was proposed in [11] to recover the energy available from the RB by dividing the driving modes to three strategies: acceleration, constant speed and braking strategy. Input signals of the algorithm are SOC of batteries, SOC of SC, vehicle speed and acceleration, while the output signal is DC-DC converter reference. The disadvantage of such PSA is that it does not release enough energy from SC to free capacity of SC to absorb energy from RB. Also, it does not take the factor of speed transient variation in the constraints to avoid battery degradation.

A fuzzy-based PSA was implemented in [12]. A fuzzy management system has been realized whenever the battery SOC is too low and in order to improve vehicle's autonomy, limit the power supplied by the battery pack and allow only degraded dynamic performance in terms of velocity and acceleration. However, this is considered a drawback, as it limits the performance of EV when a high torque is needed.

In [5], an optimization framework is used to compute the discharge current of the HESS; but the driving cycle profile is not detected accurately. Simulation results have shown it can stabilize the battery current in EV. However, its main disadvantage is that it gives priority to minimize battery current and increases its stability resulting in an SC overstressed and consequently, SC provides all the load power in some periods decreasing SOC to very low levels.

The fast Fourier transform (FFT)-based PSA was also applied in [13], where the frequency spectrum of the power demand was obtained, and based on a cut off frequency, the battery supplies the low frequency components of the power profile, whereas the SC will handle the higher frequency

components. The drawback of that approach is that the cut off frequency of the filter is not updated with the change of the driving cycle.

A wavelet-based PSA was suggested in [14] for the urban dynamometer driving cycle. The battery feeds a smooth power profile along with reduced power levels, while the SC serves to meet the dynamic power transients but the main drawback is that the power delivered by battery still not regular and has a noticeable steep variation which causes degradation in battery lifetime cycles (BLTC). The Discrete Wavelet Transform (DWT) as a time-frequency filter is also incorporated with nonlinear auto-regressive neural network time series prediction model to develop a real time PSA for battery-SC hybrid vehicles in [15]. However, this approach does not reach to optimum regular discharging current of battery which can reflect significantly on BLTC and battery thermal performance (BTP). Implementing a PSA based on combining WT, neural network (NN) and fuzzy logic was also proposed in [16]. In which, the dataset obtained from WT was used to offline train a NN to predict the low frequency power demand for the battery while the high frequency component is online calculated and fed by the SC and finally the fuzzy logic-based controller was developed to keep the SC voltage within suitable range.

Despite of the huge previous works which propose different PSAs, most of them have focused on enhancing the SOC of the battery and to reduce the variation of battery discharging current to a fewer amount, however the battery discharging current can be smoothed more and get better effects not only on SOC but also on BLTC and BTP.

In this paper, HESS of lithium-ion battery and SC is applied to optimize BTP and enhance BLTC. The principal contribution is to develop a PSA to manage power sharing between battery and SC in EV using WT with different decomposition levels of power demand signal to reach the optimum BTP with extended BLTC. This work aims to stabilize the battery current to a regular discharging current, in which, the low frequency component of the power demand was attributed to the battery while the high frequency component was attributed to the SC. Besides, the driving cycle is classified by pattern recognition NN technique to identify the nearest driving behavior to help in detecting the appropriate power sharing. The algorithm was evaluated by using modified simulation model from ADVISOR toolbox under different drive cycles: Urban Dynamometer Driving Schedule (UDDS) profile, Highway Fuel Economy Test (HWFET), New York City Cycle (NYCC), Los Angeles 1992 (LA92) and new European driving profile (ECE).

2. System Description and Modelling

As mentioned before, the proposed HESS incorporates the lithium battery with SC. The block diagram of the studied system is shown in Fig. 1. In the following subsections, the configuration design of HESS was fully described in addition to the mathematical models of HESS components to be used in simulation and validation of the proposed power sharing algorithm (PPSA).

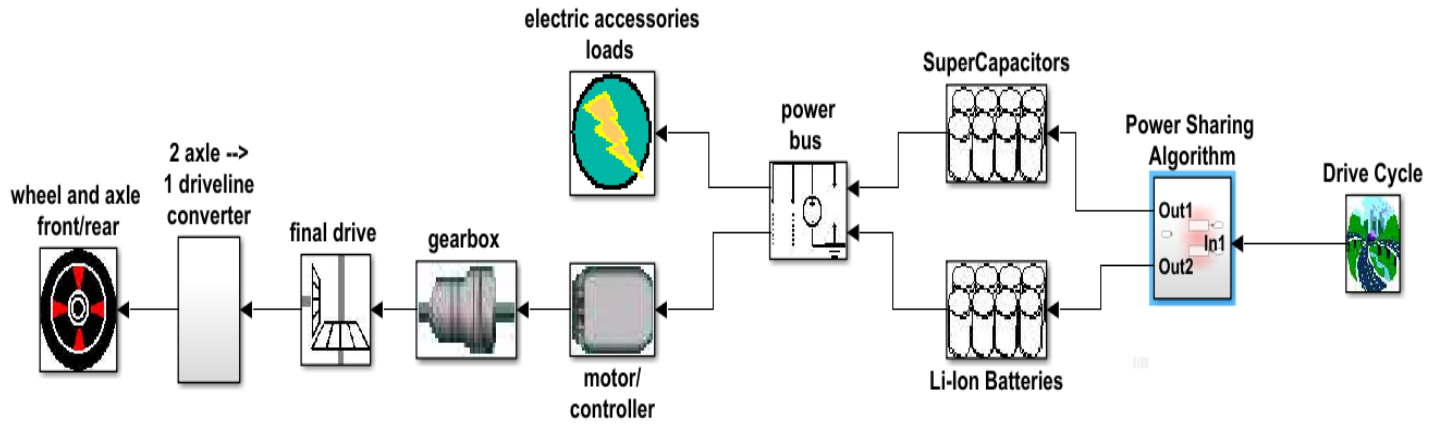


Fig. 1. System block diagram.

2.1. Configuration design of HESS

The configuration design of the HESS affects the performance and efficiency of the HESS, so it should be selected according to the objectives and priorities specified by the designer. Three forms of HESS can be considered based on the schemes reported in the literature: passive, fully active, and semi-active configurations [6].

- In passive configuration, the battery and SC are connected in parallel to the DC bus without using any converters. This configuration has the lowest cost but the SC performance is not optimum. It also, does not include any control algorithm.
- In fully active configuration, the size, cost and efficiency are compromised. It is controlled by using two bidirectional DC/DC converters and an additional control circuit.
- The semi-active HESS comprises only one bidirectional DC/DC converter and grants a good solution which compromises both system performance and cost.

The semi-active HESS was applied in this paper work with only one converter so its cost is cheaper than fully active configuration, besides the converter provides better performance to control the power flow than the passive configuration [17]. For this configuration, the battery is directly connected to the DC bus and the SC is connected to the bidirectional converter so the SC acquires RB power.

2.2. Modelling of Battery

Open-circuit voltage model of the batteries was utilized in this paper, which includes the controlled dc voltage source E_{bat} in series with the internal resistor R_{bat} . The model that represents the dynamics of the battery over the driving cycle as in ADVISOR model is mathematically shown in eqns. (1)-(3) [18].

Battery SOC minimum and maximum values are chosen to be 20, 80 % to keep up battery lifetime [19], where battery initial SOC is selected to be at 100%. Because of the limited representation of battery SOC modeling in ADVISOR toolbox, the effect of battery aging

on the value of State of Health (SOH_{bat}) and also the effect of battery state of charge (SOC_{bat}) on SOH_{bat} is added to the model as, at the sample number i , as revealed in eqns. (4)-(5) [20], [19].

$$V_{bat} = E_{bat} - I_{bat} \times R_{bat} \tag{1}$$

$$P_{bat} = V_{bat} \times I_{bat} \tag{2}$$

$$I_{bat} = \frac{E_{bat} - \sqrt{(E_{bat}^2 - 4R_{bat} \times P_{bat})}}{2R_{bat}} \tag{3}$$

$$SOC_{bat}(i) = SOC_{bat}(i - 1) - \frac{I_{bat}(i)}{3600 \times SOH_{bat}(i) \times C_{bat}} \tag{4}$$

$$SOH_{bat}(i) = SOH_{bat}(i - 1) - Z_{cy} \times [SOC_{bat}(i) - SOC_{bat}(i - 1)] \tag{5}$$

Where V_{bat} is the battery output voltage, E_{bat} is the battery dc voltage source, I_{bat} is the charging or discharging current of the battery, R_{bat} is the battery internal resistance, P_{bat} is the power output or input to the battery, SOC_{bat} is battery state of charge, SOH_{bat} is battery State of Health, C_{bat} is the rated capacity of the battery and Z_{cy} describes the cycling ageing rate of the battery.

2.3. Modeling of battery lifetime cycles (BLTC)

In paper work, we focus on the effect of steep variation of discharging currents of battery under operating temperature, the aging, and degradation of BLTC. The battery model in ADVISOR does not include BLTC, thus the BLTC was modeled and added.

As discussed in [21], BLTC depends on the operating temperature of cell (T), depth of discharge (DOD), discharging and charging current rates. The evolution of cycle number is a function of operating temperature and can be designated by a polynomial relationship of 3rd order as in eqn. (6).

$$CL(T) = a \times T^3 - b \times T^2 + c \times T + d \tag{6}$$

Where CL denotes battery lifetime cycles while T defines the operating temperature in °C. Such empirical

equation can be derived using the least-square fitting method, and the coefficients a , b , c and d were derived as described in [21] from experimental results.

2.4. Modeling of the supercapacitor (SC)

By using a similar equivalent circuit described for modeling the battery, the SC can be modeled using the following eqns. (7)-(9) [18]:

$$I_{SC} = \frac{V_{SC} - \sqrt{(V_{SC}^2 - 4R_{SC} \times P_{SC})}}{2R_{SC}} \tag{7}$$

$$V_{SC}(i + 1) = V_{SC}(i) - I_{SC} \times \frac{\Delta t}{C_{SC}} \tag{8}$$

$$SOC_{SC}(i) = \frac{(Q_{rated} - \sum_{i=1}^i I_{SC}(i))}{Q_{rated}} \tag{9}$$

Where I_{SC} is the charging or discharging current of the SC, R_{SC} is its internal resistance, P_{SC} is the power output or input of the SC. While, $V_{SC}(i)$ is the controlled dc voltage source, C_{SC} is the capacity of the SC, Δt is time interval, SOC_{SC} is the SOC of SC, Q_{rated} is the rated charge of SC in Coulombs which equals the product of the rated voltage and its capacitance.

The minimum and maximum values SC SOC are chosen to be 5%, 100 % to avoid voltage drop on DC-DC converter [19].

2.5. DC Bus Voltage and DC-DC Converter Constraints

The DC bus voltage V_{DC} is achieved related to the voltage of one battery V_{bat} through the number of series batteries as shown in eqn. (10). The duty cycle of the DC-DC converter $D(i)$ is calculated by applying eqn. (11) [19].

$$V_{DC} = V_{bat} \times N_{SB} \tag{10}$$

$$D(i) = \frac{V_{bat} \times N_{SB}}{V_{sc} \times N_{SSC}} \cdot \gamma(i) + \frac{V_{sc} \times N_{SSC}}{V_{bat} \times N_{SB}} \cdot [1 - \gamma(i)] \tag{11}$$

Where N_{SB} and N_{SSC} describe the number of series batteries, and series SC units respectively. The binary variables $\gamma(i)$ take the value of 1 in case of motoring and zero value in case of regenerating.

3. Proposed power sharing algorithm (PPSA)

As discussed before, the paper introduces a scheme to manage power sharing between battery and SC in EV using WT with different decomposition levels of power demand signal. The proposed strategy includes two parts, one is achieved offline while and the other is a real-time.

- In the first part, the datasets of selected drive cycles are used to train the NN offline.
- In the second part, the trained neural network model combined with a wavelet controller is implemented in a real-time system. The NN recognizes the input drive cycle by checking its data at specific interval

(set by the designer in terms of time or distance), and then the proper number of decomposition levels is detected based on such drive cycle profile. Consequently, the wavelet based PPSA is applied to determine the battery power while the remaining demand power is fed by the supercapacitor.

The procedures of PPSA are summarized in Fig. 2 and then described in details in next subsections.

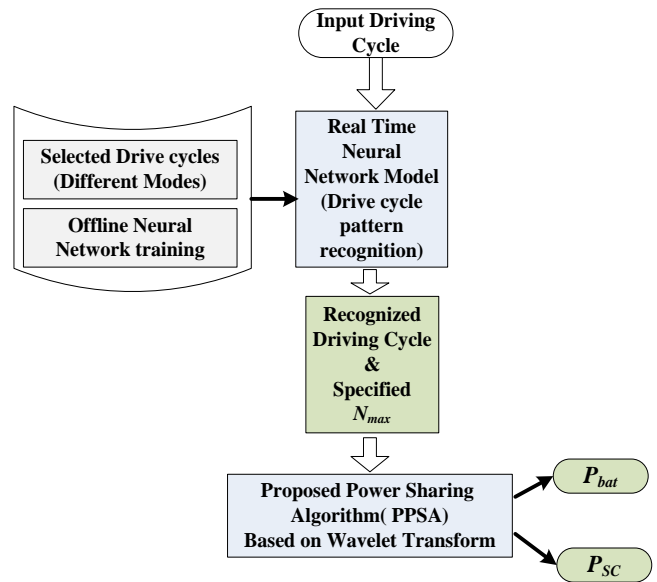


Fig. 2: Schematic diagram to implement the overall proposed scheme

3.1. Selecting optimum mother wavelet

As known, DWT is an effective technique to transform signals from time domain and decompose them in time-frequency domain without hiding the details of the signals that are usually hidden in the frequency domain. The first step is to choose the best mother wavelet, so number of factors is considered according to the application. For EV application, it is appropriate to choose the Haar mother wavelet, described in Fig. 3, because [22]:

- It has the smallest filter length in time domain with simple mathematical formulation, which is very interesting for PSA in EV for real-time algorithm, where rapid mathematical implementation is needed.
- For the approximation signal, the values are constant at fixed intervals of time (related to the decomposition level), which is optimum for slow response source such as the battery in our case.

3.2. Determining optimum number of decomposition levels

In several reported works in literature, it is found that the number of decomposition levels was selected in an arbitrary procedure according to the required details, which desired to be extracted from the signal. For example, it is found that the number of levels was selected to be three, as in [23], four in [24], or five decomposition levels in [19].

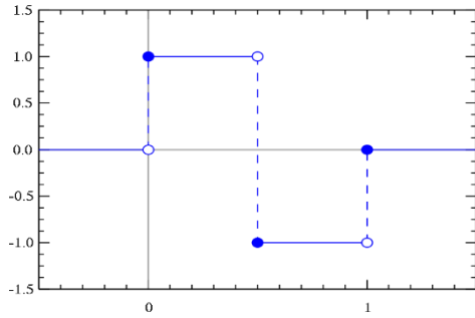


Fig. 3: Haar mother wavelet

On the other hand, in this paper, as the low frequency component of the power demand is related to the battery while the high frequency component is related to the SC, the number of decomposition levels is chosen based on the maximum allowable wavelet decomposition levels (N_{max}) depending on the number of samples N_i according to the drive cycle profile. Such value of the maximum allowable wavelet decomposition levels is calculated using eqn. (12) [25], (e.g., UDDS profile has $N_i=1370$ samples, and thus N_{max} will be 10).

$$N_{max} = \log_2 N_i \tag{12}$$

Therefore, PPSA based on DWT is implemented to here to decompose the demand power signal (P_D) of EV for any driving cycle profile using developed MATLAB M-file, where decomposition and reconstruction process are done at N_{max} decomposition levels. Therefore, the approximation decomposed signal is assigned to the battery and the summation of all detailed decomposed signals, which contains the high frequency components, is assigned to the SC. The following eqns. (13)-(15) describe that:

$$P_D = P_{bat} + P_{SC} \tag{13}$$

$$P_{bat} = a_{N_{max}} \tag{14}$$

$$P_{SC} = d_1 + d_2 + d_3 + \dots + d_{N_{max}} \tag{15}$$

Where P_{bat} describes the delivered power by battery, P_{SC} is the power delivered by SC, $a_{N_{max}}$ is the approximation signal at level N_{max} and $d_{N_{max}}$ denotes the detail signal at same N_{max} level.

To ensure that the approximation signal frequency will be in the interval of characterization frequency of the battery fc within range $[0, fc]$, the decomposition level must exceed the minimum limit specified by the following eqn. (16) [22]:

$$N_{min} = \left\lceil \frac{\log \frac{fs}{fc}}{\log 2} - 1 \right\rceil \tag{16}$$

Where fc is the battery characterization frequency that can be calculated from eqn. (17) based on the specific power (ρp in W/kg) and the specific energy (ρe in J/kg) of the battery [26], while fs describes the sampling frequency.

$$fc = \frac{\rho p}{\rho e} \tag{17}$$

For Li-Ion batteries, ρe ranges 30-300 Wh/kg, and ρp ranges 8-2000 W/kg [27]. In paper work, the implemented Li-Ion battery is SAFT 6 Ah LI-Ion Cells which has ρe of 64 Wh/kg and ρp of 1500 W/kg [28]. Accordingly, $fc=0.0065$ Hz.

The power demand in paper work is discretized with sampling time T_s of 1 second. Consequently, as the sampling frequency fs is 1 Hz, thus the estimated numerical value of N_{min} equal 6.265, therefore N_{min} is approximated to the integer number of 6 levels.

3.3. Driving cycles pattern recognition using neural networks (NNs)

Neural networks (NNs) techniques are properly used for identification, classification and pattern recognition in different applications such as roadway type detection and traffic congestion prediction [29].

In this paper, for more accurate specifying the appropriate maximum decomposition level depending on the driving cycle profile, NN is developed, trained and tested by datasets of different drive cycle profiles. A two-layer feed-forward network, with sigmoid activation function for neurons work, can recognize the correct driving cycle, given that adequate neurons are implemented in its hidden layer. The training used for this network was scaled conjugate gradient back propagation.

Accordingly, Table 1 shows a list of three driving cycles used for training the NN in this study, which are Urban Dynamometer Driving Schedule (UDDS), Highway Fuel Economy Test (HWFET), and new European driving cycle (ECE). Three different driving cycles as shown in Table 2, are also used for testing the network: SC03 Supplemental Federal Test Procedure (SC03), US06 Supplemental Federal Test Procedure (US06), Extra Urban Driving Cycle (EUDC) [30], [31]. It is worth mentioning that these driving cycles were chosen to form a diverse group of conditions. Some were highway driving cycles, some were urban driving cycles, and some belong to modal cycles (there are parts in these cycles where the speed is constant).

Using MATLAB neural pattern recognition tool, the input matrix used to train the NN has 3 rows, containing the six statistical parameters for the cycle values mentioned in Table 1. The desired output matrix called the target matrix was 3x3 matrix. The first row has a '1 0 0' for UDDS driving cycle, '0 1 0' for HWFET driving cycle and '0 0 1' for ECE driving cycle.

The network is generated with performance cross entropy (CE) value equals 3.61e-07 and 0 percent error (% E) which means good classification with no misclassification error. After training the NN with inputs and targets shown in Table 1, the NN was tested with the same inputs to check whether it could produce the targets. Then the network is tested with three inputs matrices representing the cycles mentioned in Table 2. The results are summarized in Table 3. According to results, both SC03 cycle and US06 cycle are classified to be near UDDS cycle. On the other hand, the EDUC cycle is classified to be near ECE cycle.

Table 1: Training-driving cycles

Parameter	Cycle		
	UDDS	HWFET	ECE
Max. Speed km/h	91.25	96.4	50
Avg. Speed km/h	31.51	77.58	18.26
Max. Acc. m/sec ²	1.48	1.43	1.06
Max. Deacc. m/sec ²	-1.48	-1.48	-0.83
Avg. Acc. m/sec ²	0.5	0.19	0.64
Avg. Deacc. m/sec ²	-0.58	-0.22	-0.75

Table 2: Test driving cycles

Parameter	Cycle		
	SC03	US06	EUDC
Max. Speed km/h	88.19	129.23	120
Avg. Speed km/h	34.51	77.2	62.44
Max. Acc. m/sec ²	2.28	3.76	0.83
Max. Deacc. m/sec ²	-2.73	-3.08	-1.39
Avg. Acc. m/sec ²	0.5	0.67	0.38
Avg. Deacc. m/sec ²	-0.6	-0.73	-0.93

Table 3: Neural networks classification results

Training			
UDDS cycle	UDDS	HWFET	ECE
CE	3.33E-07	4.89	4.78
%E	0	100	100
HWFET cycle	UDDS	HWFET	ECE
CE	4.53	5.14E-07	5
%E	100	0	100
ECE cycle	UDDS	HWFET	ECE
CE	4.87	5.05	2.35E-07
%E	100	100	0

Test			
SC03 cycle	UDDS	HWFET	ECE
CE	3.37E-06	3.83	5.6
%E	0	100	100
US06 cycle	UDDS	HWFET	ECE
CE	4.85E-06	3.71	5.64
%E	0	100	100
EUDC cycle	UDDS	HWFET	ECE
CE	4.61	1.08	1.31E-02
%E	100	100	0

4. Analysis of simulation results and discussion

To validate the PPSA performance, system simulation was established according to the power demand of the hypothetical small car EV (VEH_SMCAR-EV) using ADVISOR software libraries MATLAB/Simulink based simulation program.

The main parameters of VEH_SMCAR-EV, batteries and SC are shown in Table 4, which are taken from the data files on ADVISOR tool depending on the achieved testing at National Renewable Energy Laboratory (NREL).

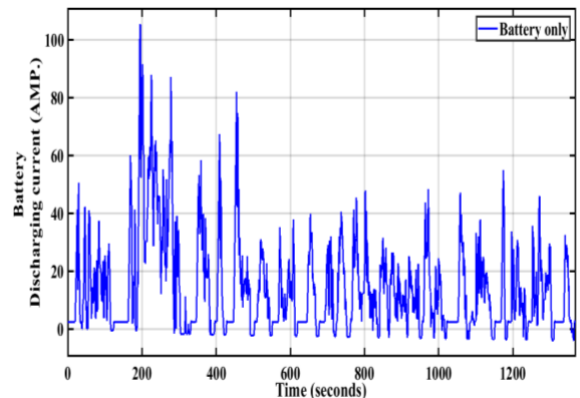
Table 4: Main parameters of VEH_SMCAR-EV

EV total mass	866 kg
Motor	32 kW (PMSM)
Batteries	Saft Lithium-Ion battery 3.2 V, 6 Ah cells, 25 modules in series
SC	Maxwell PC2500 SC 2.5 V, 2500 F, 32 modules in series with 6 modules in parallel 500000 duty cycles 10-year life capability

The series number of batteries modules is determined depending on the DC bus voltage, which is ranged from 200 to 600 volts [32] according to system specifications, as the battery is connected directly to the bus. While the parallel modules number is assumed one as it is desirable according to the distance range requested by the designer. The series and parallel number of supercapacitor modules are chosen according to [19], where the size of SC is optimized to minimize cost, weight, and volume and maximize the battery life cycle.

4.1. Evaluating battery & SC discharge current profile

When the battery is only used as energy storage power source, the discharge current consumed to meet the power demand for UDDS profile will have steep variations with high transients because of the variation in speeds at acceleration and braking as shown in Fig. 4.

**Fig. 4:** Battery discharging current for UDDS profile when using battery only

When using the SC as a secondary power source, and applying the PPSA based on DWT to meet the high frequency components of the power demand, the battery discharge performance is evaluated. Decomposition and reconstruction process are done at different decomposition levels, starting from three levels to N_{max} of ten levels for UDDS profile to validate the effectiveness of using the maximum decomposition level and its effect on BLTC and BTP. In fact, the limitation for N_{min} levels will also be investigated by applying lower levels of decomposition as used in literature (three & five levels as examples) to check the effects on BTP & BLTC. The battery discharge current

for UDDS profile is shown in Fig. 5 for different wavelet decomposition levels: 3, 5, 6 (N_{min}) & 10 (N_{max}).

It is clear from Fig. 5-d that for N_{max} at ten levels, the current is constant which is considered the perfect performance for the battery from the point of view of the thermal operating temperature and BLTC as will be shown in the next section.

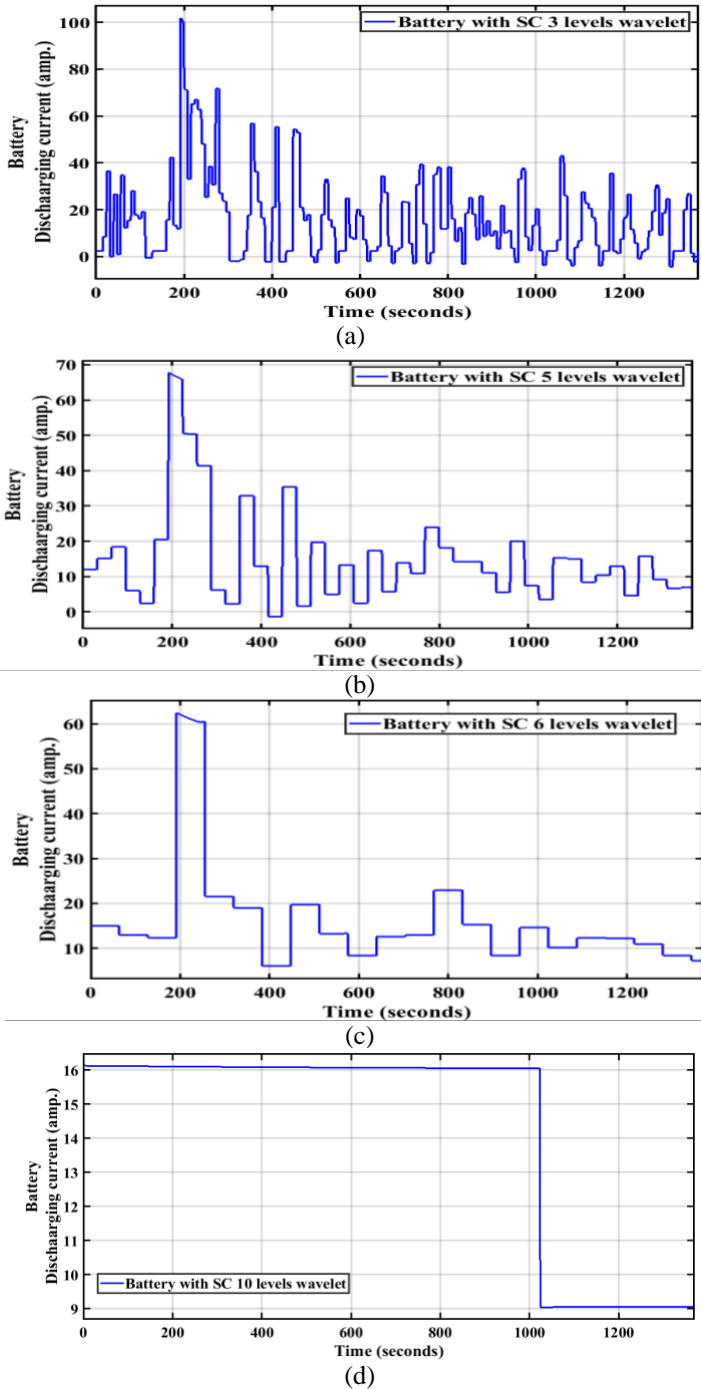


Fig. 5: Battery discharging current for UDDS profile when using battery-SC HESS at different decomposition levels (a) At 3 levels wavelet decomposition, (b) At 5 levels wavelet decomposition, (c) At 6 levels wavelet decomposition, (d) At 10 levels wavelet decomposition

Discharging currents for the SC at same decomposition levels for UDDS profile are also illustrated in Fig. 6. Because of the fast time response of the SC and its flexibility to send/receive power at a fast rate, it is deduced that SC is convenient to feed this amount of power to EV.

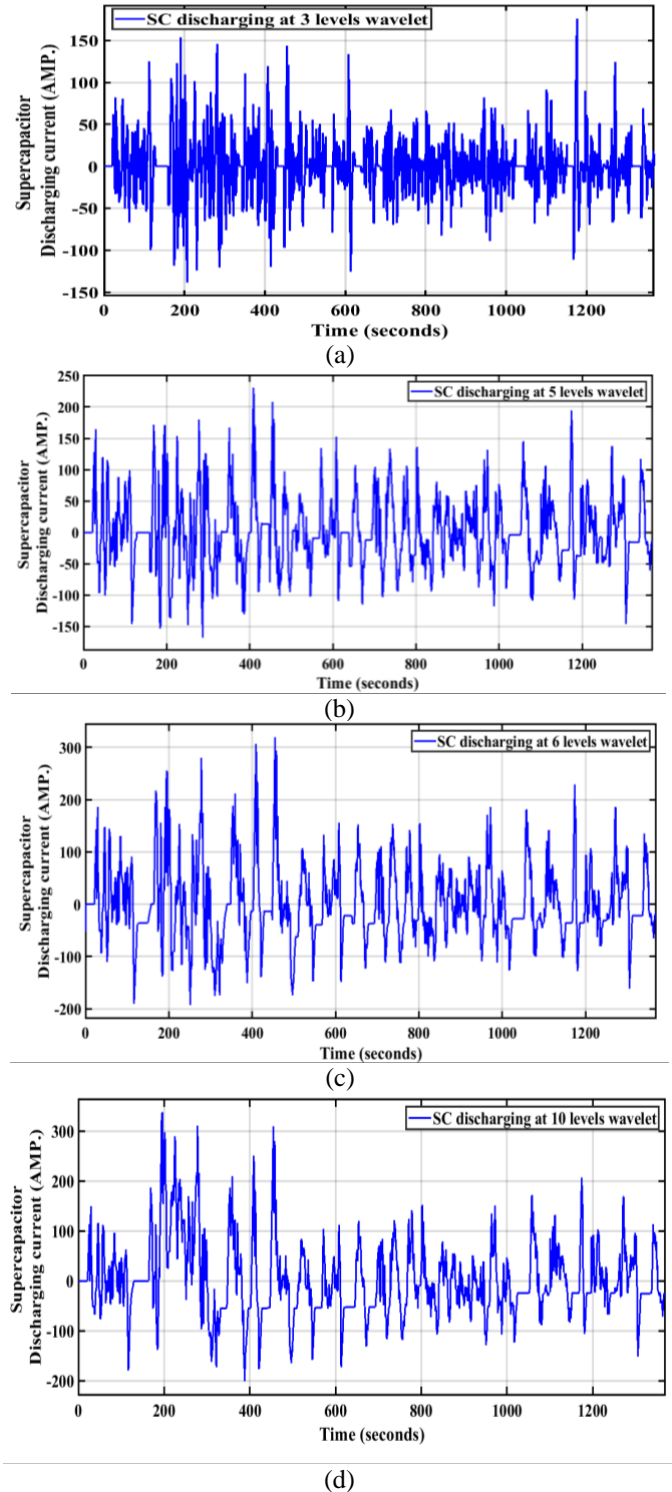


Fig. 6: SC discharging currents for UDDS profile when using battery-SC HESS at different decomposition levels (a) At 3 levels wavelet decomposition, (b) At 5 levels wavelet decomposition, (c) At 6 levels wavelet decomposition, (d) At 10 levels wavelet decomposition

4.2. Evaluating battery thermal performance (BTP)

Depending on the geographic regions and climatic zones, the operation range of EV is possible between -30 °C and 60 °C [33], [34], while the best temperature range of ambient temperature for Li-ion batteries is between 25 °C and 40 °C. Table 5 describes the influence of temperature on the working principle of Li-ion batteries [33].

The operating temperature and the heat generated from the battery were expressed as follows in eqn. (18):

$$q = I_{bat}^2 \times R_{bat} - I_{bat} \times T \times \frac{dE}{dT} \tag{18}$$

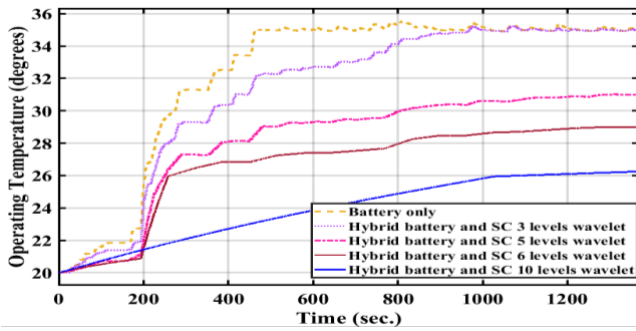
Where q is the heat generated, R_{bat} is the total resistance of the battery, I_{bat} is the discharging/charging current, $I_{bat}^2 \times R_{bat}$ is the joule heat caused by internal resistance of Li-ion battery and the polarization heat caused by the loss of mass transfer, $I_{bat} \times T \times \frac{dE}{dT}$ is the reaction heat on anode and cathode (thermal entropy change) [34].

For UDSS drive cycle profile, Fig. 7.a illustrates the battery thermal performance when using the battery only compared with HESS of battery/SC and applying PPSA. As shown, the battery suffers from highest operating temperature when the battery is only used as a storage system; it reaches to about 35 °C for one cycle of UDSS with 1370 seconds. On contrary, it only reaches to about 25.6 °C when the battery is combined with SC and applying the PPSA with 10 decompositions levels.

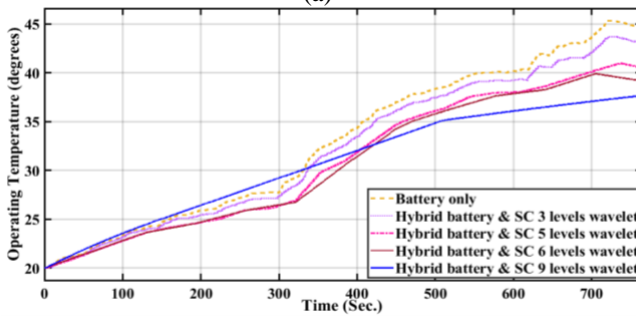
The same procedure is repeated for different profiles:

- HWFET with N_{max} of 9 levels,
- NYCC with N_{max} of 9 levels,
- LA92 with N_{max} of 10 levels and
- ECE with N_{max} of 7 levels.

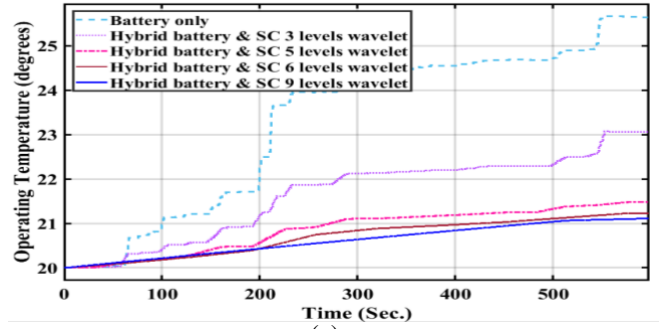
The results are illustrated in Fig. 7.b, c, d and e respectively, where the best BTP is achieved for all cycle profiles at the corresponding N_{max} .



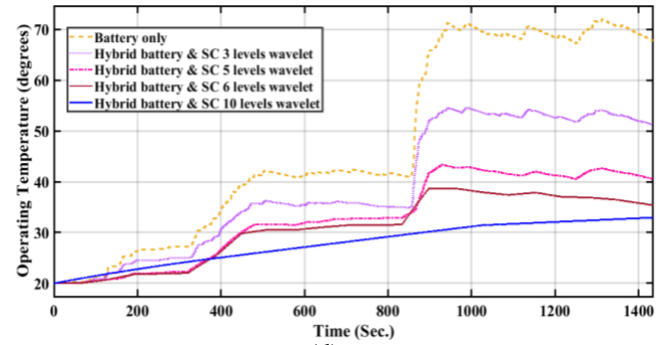
(a)



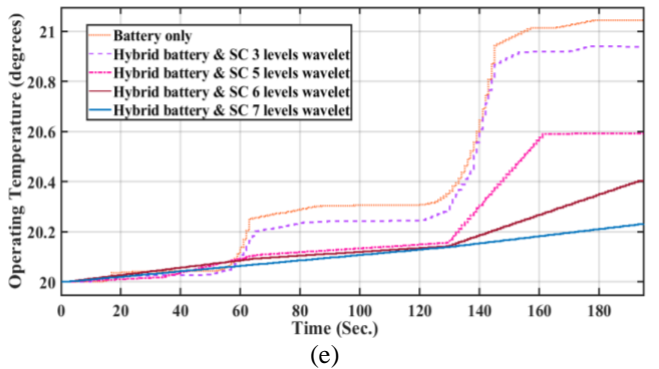
(b)



(c)



(d)



(e)

Fig. 7: BTP for different profiles when using only battery compared to HESS and applying PPSA at different wavelet decomposition levels

(a) For UDSS profile, (b) For HWFET profile, (c) For NYCC profile, (d) For LA92 profile (e) For ECE profile

Table 5: Temperature influence on batteries [33]

Low temperature (< 0 °C)	- Capacity drop - Internal resistance increase
High temperature (> 40 °C)	- Internal resistance decreases - Accelerated aging phenomena - Higher self-discharge - Decomposition of electrolyte - Thermal runaway, safety considerations - Reduced BLTC

4.3. Evaluating battery lifetime cycles (BLTC)

As discussed before, ADVISOR tool battery block does not have any mathematical model for BLTC representation so a mathematical model was added to the simulation to validate the PPSA. The data of BLTC was used for Lithium-ion battery but with different positive electrodes

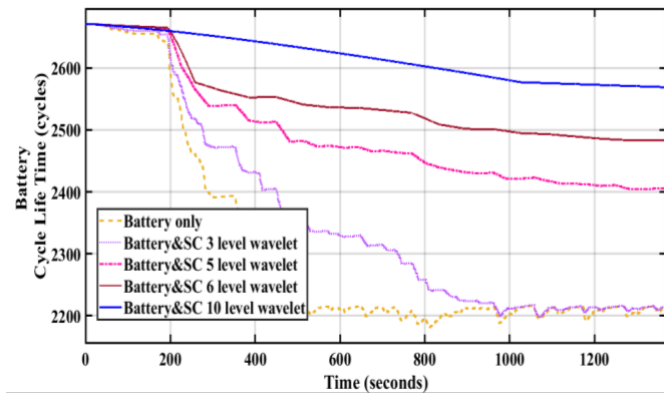
(Lithium cobalt oxide instead of Lithium iron phosphate oxide); this replacement was done because of the lack of data for BLTC model for Lithium cobalt oxide, and according to [35], it will not affect the accuracy of results referring to battery aging.

Extension increment in BLTC is investigated at different wavelet decomposition levels for UDDS profile to show the superiority of using the maximum decomposition level allowed. The simulations are also carried out for different driving profiles to assure the validity of using the developed algorithm.

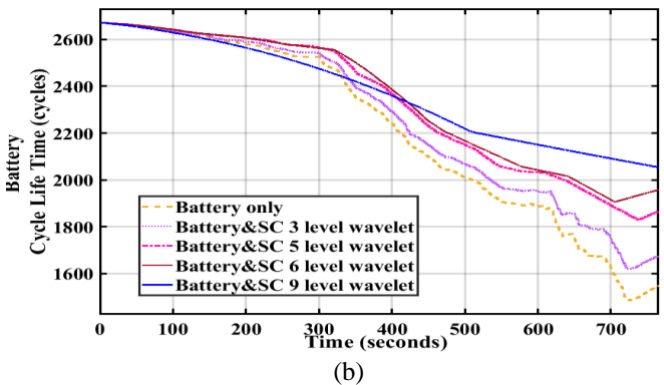
As discussed before in eqn. (6), the coefficients a , b , c and d are derived from the experimental results in [21]: $a = 0.0039$, $b = 1.95$, $c = 67.51$, $d = 2070$. By applying such values, BLTC is compared when using the battery only compared with using the HESS of battery-SC and applying PPSA for different drive cycles as revealed in Fig. 8.

For example, for UDDS drive cycle profile (Fig. 8.a), the battery $CL(T)$ reaches about 2213 cycles while it increases significantly to about 2585 cycles with about 372 cycles rise for HESS of battery-SC and applying PPSA at N_{max} decomposition levels.

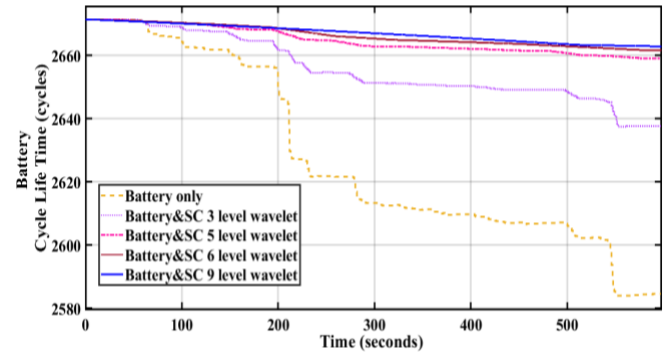
Figures 8.b, c, d and e have also ensured best $CL(T)$ during different profiles of HWFET, NYCC, LA92 and ECE respectively.



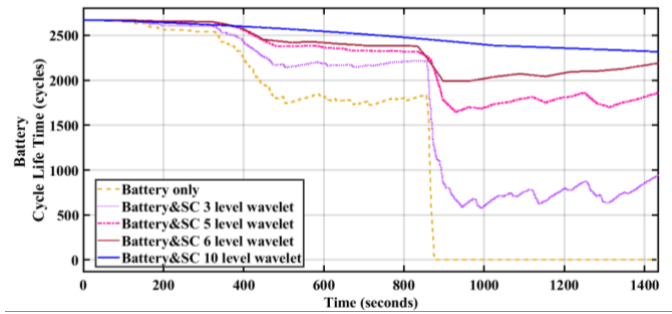
(a)



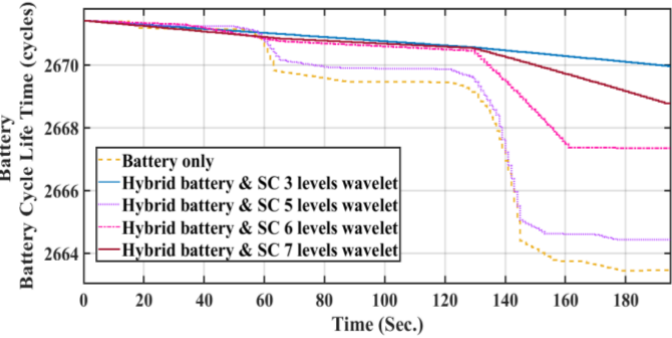
(b)



(c)



(d)



(e)

Fig. 8: BLTC when using only battery compared to HESS and applying PPSA at different decomposition levels (a) For UDDS profile, (b) For HWFET profile, (c) For NYCC profile, (d) For LA92 profile (e) For ECE profile

4.4. Evaluating SOC for battery and SC

The SOC of lithium battery is also investigated for UDDS profile for the two cases: when only using the battery and when using the HESS of battery/SC and applying PPSA at N_{max} decomposition levels as illustrated in Fig. 9. It is clear that applying HESS via PPSA extends the range of battery capacity.

Moreover, for UDDS drive cycle, the SOC of SC is compared when applying PPSA at three levels & N_{max} wavelet decomposition levels. As shown in Fig. 10, when applying N_{max} of 10 levels, the SOC of SC decreases considerably to about 0.7 because of feeding the transient power and recovered to about 0.88 due to RB power harvesting. On the other hand, when applying three levels of decomposition, the SOC of SC is enhanced to 0.98 with slight variations.

It is supposed that at N_{max} , the SC is loaded more than at three levels decomposition. This is because of feeding

more high frequency transients' components of the power demand but SC is still kept at normal loading as SC is not overstressed and the SOC is within acceptable range.

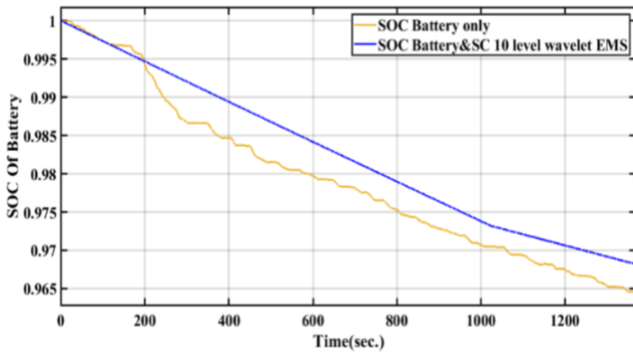


Fig. 9: Battery SOC for UDDS profile when using only battery compared to HESS and applying PPSA at N_{max} decomposition levels

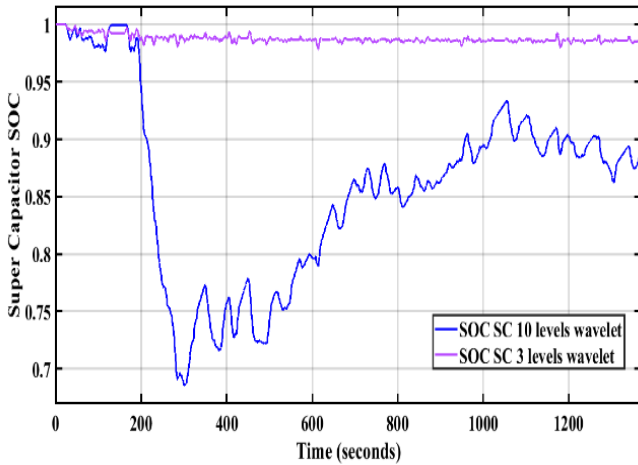


Fig. 10: SC SOC for UDDS profile when applying PPSA at three & N_{max} wavelet decomposition levels

4.5. Results discussion for optimum selection of decomposition levels

The verification of using the maximum number of decomposition levels as the optimum selection for both BTP & BLTC of the battery is summarized in this section. A detailed comparison is carried out to investigate the effect of the frequency band for the wavelet approximation signal fed to the battery on BTP, BLTC, battery SOC and SC SOC for UDDS drive cycle. All decomposition levels from three to ten are investigated; the wavelet approximation frequency ranges (a3, a4, a5, a6, a7, a8, a9 and a10) are compared against the characterization frequency of the implemented Li-Ion battery of 0.0065 Hz as shown in Fig. 11. Table 6 summarizes the accomplished results. As shown, the wider frequency range of the approximation out of the characterization frequency range, the worse values of BTP, BLTC, battery SOC and SC SOC are achieved.

For different drive cycle profiles, Table 7 summarizes the achieved results for applying PPSA a N_{max} decomposition levels compared to using N_{min} . As shown, both BTP & BLTC have improved in all profiles and

especially in UDDS, LA92 profiles which are characterized by great variations with frequent stops. In fact, BTP has improved in such profiles by 4% and 8.76% when using N_{max} instead of N_{min} , while BLTC has enhanced significantly by 13.28% and 12.38% when applying UDDS and LA92 respectively.

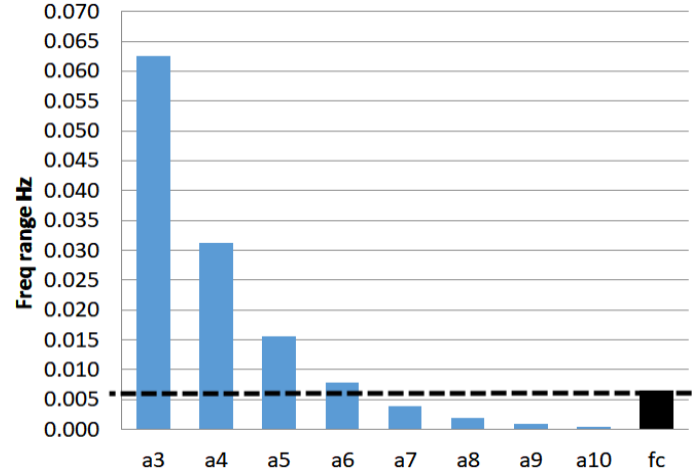


Fig. 11: Frequency ranges of wavelet approximation for decomposition levels from three to ten

Table 6: Comparative results for different decomposition levels and applying PPSA for UDDS drive cycle

No. of decomposition levels	Parameter			
	BTP	BLTC	Battery SOC	SC SOC
3	35	2213	0.9635	0.983
4	34.5	2240	0.9642	0.98
5	31	2405	0.9656	0.954
$N_{min} = 6$	29	2484	0.9658	0.94
7	27.4	2537	0.9659	0.864
8	26.7	2557	0.9659	0.799
9	26.4	2565	0.9664	0.833
$N_{max} = 10$	25.6	2585	0.968	0.887

Table 7: Comparative results for different drive cycle profiles and applying PPSA with N_{max} decomposition levels compared to N_{min}

Parameter	Drive cycle profile				
	UDDS	HWFET	NYCC	LA92	ECE
N_{max}	10	9	9	10	7
N_{min}	6	6	6	6	6
BTP at N_{max} (°C)	25.6	37.7	21	31.5	20.2
BTP at N_{min} (°C)	29	39.2	21.23	35.4	20.4
BLTC at N_{max} (cycles)	2585	2053	2663	2383	2670
BLTC at N_{min} (cycles)	2484	1957	2661	2191	2663

5. Conclusion

A proposed power-sharing algorithm (PPSA), using DWT to decompose the EV power demand signal at maximum number of decomposition levels, was implemented. NN is also developed to recognize the driving cycle profile to use the appropriate power sharing to achieve the best BTP and BLTC for the driving behavior and to get the best performance for the battery integrated in HESS with SC.

The simulation model of the HESS in the VEH_SMCAR-EV based on ADVISOR is established to validate the PPSA for the power-balancing strategy of power distribution. Different driving profiles (UDDS, HWFET, NYCC, LA92 & ECE) are applied to validate the effectiveness of applying maximum decomposition levels and study the effect on BTP and BLTC. The proposed algorithm proves its efficiency in decreasing the battery temperature, by controlling the power sharing between battery and SC with respect to the drive cycle profile. For UDDS, the operating temperature of lithium battery is improved much at N_{max} decomposition levels reaching to only 25.6 °C compared to 29 °C at N_{min} decomposition levels. In addition, BLTC is increased from 2484 to 2585 cycles by raising the decomposition levels from N_{min} of six levels to N_{max} of ten levels. Enhanced battery performance is also attained for other drive cycle profiles (HWFET, NYCC, LA92 & ECE) in both BTP and BLTC; it ensures the suitability of the PSSA to be applied in all drive cycle profiles.

Finally, through paper work, the following features are accomplished and highlighted:

- The aging effect of the battery at steep variations is modeled.
- The effect of speed transient variation is taken into consideration to avoid battery degradation by assigning the low frequency component of power demand to be fed from the battery.
- The dynamic performance of EV is not limited in case of sudden high velocity and acceleration as SC is feeding the high frequency components of power demand.
- The PPSA free sufficient capacity of SC to absorb RB power efficiently without the limitation of specific SOC and thus SC is not overstressed and SOC of SC is retrieved in suitable range.

Experimental test with real time hardware platform could be implemented in further research work to reveal the achieved results for such proposed PSA. Also, an additional supervisory controller could be further developed for controlling the supercapacitor voltage within a certain suitable range.

References

[1] C. C. Chan, Y. S. Wong, A. Bouscayrol and . K. Chen, "Powering Sustainable Mobility: Roadmaps of Electric, Hybrid, and Fuel Cell Vehicles [Point of View]," *Proceedings*

- of the IEEE*, vol. 97, no. 4, pp. 603 - 607, April 2009.(Article)
- [2] F. Altun, S. A. Tekin, S. Gürel and M. & Cernat, "Design and Optimization of Electric Cars. A Review of Technological Advances," in *8th International Conference on Renewable Energy Research and Applications (ICRERA)*, Brasov, ROMANIA, 2019 . (Conference Paper)
- [3] "iea.org," IEA , 2019. [Online]. Available: <https://www.iea.org/reports/tracking-transport-2019>.(Website)
- [4] I. Oukkacha, M. B. Camara and B. & Dakyo, "Energy Management in Electric Vehicle based on Frequency sharing approach, using Fuel cells, Lithium batteries and Supercapacitors.," in *7th International Conference on Renewable Energy Research and Applications (ICRERA)*, Paris,France, 2018. (Conference Paper)
- [5] M.-E. Choi and S.-. W. Seo, "Robust energy management of a battery/supercapacitor Hybrid Energy Storage System in an electric vehicle," in *IEEE International Electric Vehicle Conference*, Greenville, SC, USA, 2012. (Conference Paper)
- [6] L. Kouchachvili, W. Yaïci and E. Entchev, "Hybrid battery/supercapacitor energy storage system for the electric vehicles," *Journal of Power Sources*, vol. 374, pp. 237-248, 2018.(Article)
- [7] O. Veneri, C. Capasso and S. Patalano, "Experimental investigation into the effectiveness of a super-capacitor based hybrid energy storage system for urban commercial vehicles," *Applied Energy*, no. 227, pp. 312-323, 2018.(Article)
- [8] Z. Song, H. Hofmann, J. Li, X. Han, X. Zhang and M. Ouyang, "A comparison study of different semi-active hybrid energy storage system topologies for electric vehicles," *Journal of Power Sources*, vol. 274, pp. 400-411, 2015. (Article)
- [9] T. Zhu, R. G. Wills, R. Lot and X. Y. X. Kong, "Optimal sizing and sensitivity analysis of a battery-supercapacitor energy storage system for electric vehicles.," *Energy*, vol. 221, no. 119851, 2021. (Article)
- [10] D. Sun, . F. Lan and J. Chen, "Energy management strategy research and performance simulation for electric vehicles based on dual-energy storage system," in *6th International Conference on Information Management, Innovation Management and Industrial Engineering*, Xi'an, China, 2013. (Conference Paper)
- [11] J. Armenta, C. Núñez, N. Visairo and I. Lázaro, "An advanced energy management system for controlling the ultracapacitor discharge and improving the electric vehicle range," *Journal of Power Sources*, vol. 284, pp. 452--458, 2015. (Article)
- [12] V. Galdi, A. Piccolo and P. Siano , "A fuzzy based safe power management algorithm for energy storage systems in electric vehicles," in *IEEE Vehicle Power and Propulsion Conference*, Windsor, UK, 2006. (Conference Paper)
- [13] R. E. Araujo , R. P. de Castro, C. Pinto , P. Melo and D. Freitas, "Combined Sizing and Energy Management in EVs With Batteries and Supercapacitors," *IEEE Transactions on Vehicular Technology*, vol. 63 , no. 7, pp. 3062 - 3076, 2014. (Article)
- [14] L. Zhang , X. Hu , Z. Wang, F. Sun, J. Deng and D. Dorrell, "Multiobjective Optimal Sizing of Hybrid Energy Storage System for Electric Vehicles," *IEEE Transactions on Vehicular Technology* , vol. 67 , no. 2, pp. 1027 - 1035, 2017 . (Article)
- [15] M. Ibrahim, S. Jemei, G. Wimmer and D. Hissel, "Nonlinear autoregressive neural network in an energy management strategy for battery/ultra-capacitor hybrid electrical vehicles,"

- Electric Power Systems Research*, vol. 136, pp. 262-269, 2016. (Article)
- [16] Q. Zhang, L. Wang and G. & L. Y. Li, "A real-time energy management control strategy for battery and supercapacitor hybrid energy storage systems of pure electric vehicles," *Journal of Energy Storage*, vol. 31, no. 101721, 2020. (Article)
- [17] A. Sahbani, K. Cherif and K. B. & Saad, "Multiphase Interleaved Bidirectional DC-DC Converter for Electric Vehicles and Smart Grid Applications," *international Journal of Smart Grid - ijSmartGrid*, vol. 4, no. 2, pp. 80-87, 2020. (Article)
- [18] B. Wang, J. Xu, B. Cao and X. Zhou, "A novel multimode hybrid energy storage system and its energy management strategy for electric vehicles," *Journal of Power Sources*, vol. 281, pp. 432-443, 2015. (Article)
- [19] H. Eldeeb , A. ElSayed, C. Lashway and O. Mohammed , "Hybrid Energy Storage Sizing and Power Splitting Optimization for Plug-In Electric Vehicles," *IEEE Transactions on Industry Applications* , vol. 55 , no. 3, pp. 2252 - 2262, 2019 . (Article)
- [20] J. Xu, Mi, C. Chris, B. Cao and J. Cao, "A new method to estimate the state of charge of lithium-ion batteries based on the battery impedance model," *Journal of Power Sources*, vol. 233, pp. 277-284, 2013. (Article)
- [21] N. Omar, M. Abdel Monem, Y. Firouz, J. Salminen, J. Smekens, O. Hegazy, H. Gaulous, G. Mulder, P. V. den Bossche, T. Coosemans and J. V. Mierlo, "Lithium iron phosphate based battery – Assessment of the aging parameters and development of cycle life model," *Applied Energy*, vol. 113, pp. 1575-1585, 2014. (Article)
- [22] M. Ibrahim, S. Jemei, G. Wimmer, N. Y. Steiner, C. Kokonendji and D. Hissel, "Selection of mother wavelet and decomposition level for energy management in electrical vehicles including a fuel cell," *International Journal of Hydrogen Energy*, vol. 40, no. 45, pp. 15823-15833, 2015. (Article)
- [23] C. Zeng, H. Lian, T. Chen, Z. Cai and D. Fang, "A wavelet transform based power allocation strategy for lithium battery and ultra capacitor hybrid vehicular power system.," in *31st Youth Academic Annual Conference of Chinese Association of Automation (YAC)*, Wuhan,China, 2016. (Conference Paper)
- [24] Q. Zhang and W. Deng, "An adaptive energy management system for electric vehicles based on driving cycle identification and wavelet transform," *Energies*, vol. 9, no. 341, pp. 1-24, 2016. (Article)
- [25] M. Yang, Y. F. Sang, C. Liu and Z. Wang, "Discussion on the choice of decomposition level for wavelet based hydrological time series modeling.," *Water*, vol. 8.5, p. 197, 2016. (Article)
- [26] B. Robyns, C. Suedemont, D. Hissel, X. Roboam and B. & P. J. Sareni, *Electrical energy storage in transportation systems.*, ISTE, 2016. (Article)
- [27] S. Sabihuddin, A. E. Kiprakis and M. Mueller., "A numerical and graphical review of energy storage technologies," *Energies*, vol. 8.1, pp. 172-216, 2015. (Article)
- [28] M. Keyser, A. Pesaran, S. Oweis and G. & A. C. Chagnon, "Thermal evaluation and performance of high-power lithium-ion cells," in *16th Electric Vehicle Conference*, Beijing, China, 1999. (Conference Paper)
- [29] W. Vaz, R. G. Landers and a. U. O. Koylu, "Neural network strategy for driving behaviour and driving cycle classification," *International Journal of Electric and Hybrid Vehicles*, vol. 6(3), pp. 255-275, 2014. (Article)
- [30] "DieselNet," [Online]. Available: <https://dieselnet.com/standards/cycles>.(Website)
- [31] T. J. BARLOW, S. Latham and I. S. & B. P. G. McCrae, *A reference book of driving cycles for use in the measurement of road vehicle emissions*, TRL Published Project Report , 2009.(Book)
- [32] H. Wen, W. Xiao, H. Li and X. Wen, "Analysis and minimisation of DC bus surge voltage for electric vehicle applications.," *IET Electrical Systems in Transportation*, vol. 2(2), pp. 68-76, 2012. (Article)
- [33] R. Thomas , *Linden's handbook of batteries*, New York: McGraw-hill, 2011.(Book)
- [34] A. Samba , *Battery Electrical Vehicles-Analysis of Thermal Modelling and Thermal Management*, Brussel: Electric power. LUSAC (Laboratoire Universitaire des Sciences Appliquées de Cherbourg),MOBI (the Mobility, Logistics and Automotive Technology Research Centre), Vrije Universiteit, 2016.(PhD Thesis)
- [35] A. Barré, B. Deguilhem, S. Grolleau, M. Gérard, F. Suard and D. Riu, "A review on lithium-ion battery ageing mechanisms and estimations for automotive applications.," *Journal of Power Sources*, vol. 241, pp. 680-689, 2013. (Article)